AD-A173 608 ELECTROMAGNETIC SCATTERING FROM A HELIX(U) FLORIDA UNIV 1/1
GAINESVILLE R T WANG SEP 86 CRDEC-CR-86071
DAAG29-81-D-0100

UNCLASSIFIED F/G 20/14 NL

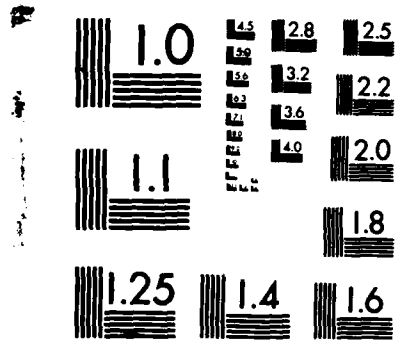

12

CHEMICAL RESEARCH, DEVELOPMENT & ENGINEERING CENTER

CRDEC-CR-86071

ELECTROMAGNETIC SCATTERING FROM A HELIX

by Ru T. Wang
UNIVERSITY OF FLORIDA
Gainesville, FL 32609

September 1986

U.S. ARMY ARMAMENT MUNITIONS CHEMICAL COMMAND

Aberdeen Proving Ground, Maryland 21010-5423

Disclaimer

The findings in this report are not to be construed as an official Department of the Army position unless so designated by other authorizing documents.

Distribution Statement

Approved for public release; distribution is unlimited.

AD-A173 608

UNCLASSIFIED

SECURITY CLASSIFICATION OF THIS PAGE

REPORT DOCUMENTATION PAGE

1a. REPORT SECURITY CLASSIFICATION UNCLASSIFIED	1b. RESTRICTIVE MARKINGS
2a. SECURITY CLASSIFICATION AUTHORITY	3. DISTRIBUTION/AVAILABILITY OF REPORT Approved for public release; distribution is unlimited.
2b. DECLASSIFICATION/DOWNGRADING SCHEDULE	
4. PERFORMING ORGANIZATION REPORT NUMBER(S) CRDEC-CR-86071	5. MONITORING ORGANIZATION REPORT NUMBER(S)
6a. NAME OF PERFORMING ORGANIZATION University of Florida 6b. OFFICE SYMBOL (If applicable)	7a. NAME OF MONITORING ORGANIZATION
6c. ADDRESS (City, State, and ZIP Code) 1810 NW 6th Street Gainesville, FL 32609	7b. ADDRESS (City, State, and ZIP Code)
8a. NAME OF FUNDING/SPONSORING ORGANIZATION CRDEC 8b. OFFICE SYMBOL (If applicable) SMCCR-RSP-B	9. PROCUREMENT INSTRUMENT IDENTIFICATION NUMBER DAAG29-81-D-0100/TCN 85-597
8c. ADDRESS (City, State, and ZIP Code) Aberdeen Proving Ground, Maryland 21010-5423	10. SOURCE OF FUNDING NUMBERS PROGRAM ELEMENT NO. / PROJECT NO. / TASK NO. / WORK UNIT ACCESSION NO.

11. TITLE (Include Security Classification)
Electromagnetic Scattering from a Helix

12. PERSONAL AUTHOR(S)
Wang, Ru T.

13a. TYPE OF REPORT	13b. TIME COVERED	14. DATE OF REPORT (Year, Month, Day)	15. PAGE COUNT
Contractor	FROM 85 08 TO 85 12	1986 September	15

16. SUPPLEMENTARY NOTATION
COR: Jerald R. Bottiger, SMCCR-RSP-B, (301) 671-2395

17 COSATI CODES		
FIELD	GROUP	SUB-GROUP
15	02	

18. SUBJECT TERMS (Continue on reverse if necessary and identify by block number)
Electromagnetic Scattering, Helical Particles, Nonspherical Particles, Microwave Scattering, ...

19. ABSTRACT (Continue on reverse if necessary and identify by block number)
Microwave measurements of scattering by a helix made from an acrylic rod are reported. All measurement results on extinction ($\theta = 0°$) and angular scattering ($10° \leq \theta (10°) \leq 170°$) are given in absolute magnitude and are displayed in comprehensive graphical form. Emphasis on measurements/discussions is based on 3 principal orientations of the helix in the beam; i.e., with the helical axis parallel to the incident $\vec{k}$, $\vec{E}$, and $\vec{H}$ vectors. Analysis is based primarily on the accuracy of the data, comparisons to scattering by an equal-volume sphere, and some of the outstanding features noted from this experiment.

20. DISTRIBUTION/AVAILABILITY OF ABSTRACT ☒ UNCLASSIFIED/UNLIMITED ☐ SAME AS RPT. ☐ DTIC USERS	21. ABSTRACT SECURITY CLASSIFICATION UNCLASSIFIED
22a. NAME OF RESPONSIBLE INDIVIDUAL TIMOTHY E. HAMPTON	22b. TELEPHONE (Include Area Code) (301) 671-2914 22c. OFFICE SYMBOL SMCCR-SPS-T

DD FORM 1473, 84 MAR 83 APR edition may be used until exhausted. All other editions are obsolete.

SECURITY CLASSIFICATION OF THIS PAGE
UNCLASSIFIED

PREFACE

The work described in this report was performed under Contract No. DAAG29-81-D-0100/TCN 85-597. This work was started in August 1985 and completed in December 1985.

The use of trade names or manufacturers' names in this report does not constitute endorsement of any commercial products. This report may not be cited for purposes of advertisement.

This report has been cleared for public release.

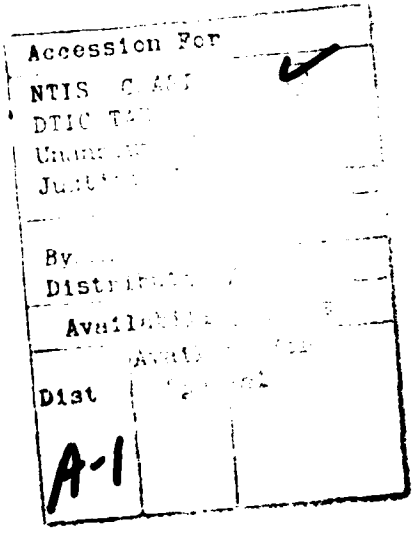

CONTENTS

ELECTROMAGNETIC SCATTERING FROM A HELIX

1. INTRODUCTION/OVERVIEW

Scattering by helical objects known to exhibit chirality (more commonly known as the optical activity [Refs. 1,2]) has been studied extensively, notably in the field of chemical physics. Investigation of Circular Intensity Differential Scattering (CIDS) of light by macromolecules, for example, provides a good understanding of the chiral structure of molecules. The helix is one of the simplest geometric forms of such chiral structures. Due to difficulties involved in the experimental study of scattering by a single helix in the optical region, especially when the helix size is comparable to the wavelength λ of the radiation, the microwave analog technique [5,6] has been used for this research due to its remarkable advantages in simulating single-particle scattering.

1.1 Preparation of a Helix and Determination of Target Parameters.

A search was conducted for materials suitable for construction of a helical target. The target medium should (A) allow the penetration of microwaves. Thus, metals had to be ruled out. (B) It should be mechanically feasible to form a helix of at least 6 turns, with a size comparable to λ=3.18 cm, and of sufficient rigidity so that it could be suspended/oriented in the beam without excessive shape deformation. (C) The scattering intensity from such a helix should be discernible against the unwanted residual background radiation. (D) At least two rectangular waveguide samples could be prepared from the same target material so that its complex refractive index m could be determined by our standard waveguide-slotted-line technique [3,4].

Acrylic plastic supplied by the Commercial Plastics and Supply Corp., 2331 Laura St., Jacksonville, Fl. 32206 was found to meet the above requirements. By virtue of its thermoplastic property and by carefully winding acrylic rods around a wooden cylinder in a household oven heated to about 400°F, several helixes of different rod-diameters were prepared. Out of these, however, only one, with 0.48 cm rod-diameter was found to have the necessary rigidity along with the other desired properties. A right-handed, 7-turn helix of 3.66 cm outer diameter and of 4.35 cm axial length was formed out of this rod, and the total volume of the helix was found to be V=14.40 cc via the application of Archimedes' water-displacement principle. From these parameters, we were also able to compute the volume equivalent and surface-area equivalent size parameters: x_v=2.979 and x_s=6.111, respectively. Finally, the measured complex refractive index was m=1.626-i0.012.

1.2 Microwave Scattering Measurements.

To avoid excessinve interruptions to our on-going DoD-URIP microwave facility upgrade program, all helix-scattering measurements were carried out using our existing old facility described in our previous Army CRDC Conference Proceedings [5,6,7]. Special PDP 11/03 computer programs were written to specifically measure and analyze the scattering data. (A) Angular scattering intensities were measured in the range $10° \leq \theta\ (10°) \leq 170°$ for 3 combinations of transmitter-receiver antenna polarizations. i_{11} denotes the intensity when both antennas are polarized vertical, i_{22} that for both antennas polarized

horizontal, and i_{12} denotes the cross-polarized scattering intensity when the transmitter polarization is vertical while the receiver is vertical. At each θ and polarization setting, the helix scatterings were measured at each of the 3 principal orientations (helical axis aligned parallel to the incident $\vec{k}$, $\vec{E}$, and $\vec{H}$ vectors). (B) $\theta = 0$ scattering data were supplemented by employing the extinction measurement technique [5,7] due to the special procedures needed in using our compensation method at $\theta = 0$. In addition to the above 3 principal helix orientations, we could also measure the scattering at 34 more orientations so that the subtle effects of particle orientations on light obscuration as well as the scattering averaged over random orientations could also be visualized.

One of the marked advantages of our microwave technique over others is in the use of the compensation technique: In the absence of a target, we can cancel the unwanted background whose magnitude can be comparable, or even larger than the scattered signal. When the target is brought into the beam, the resulting off-balance is the true scattered signal to be measured. Furthermore, by repeating the same measurement for one or two standard targets of known scattering magnitude in quick succession, the absolute magnitude of the scattering can also be calibrated. The quality of this compensation technique (or null technique), however, is judged by how small the residual uncancelled background remains and how long the compensation stays stable (which should be longer than a typical measurement run time). This is one of the major criteria with which we also judge the accuracy of measurement results.

2. EXPERIMENTAL RESULTS AND DISCUSSIONS

2.1 $\theta = 0°$ Measurements.

Scattering from the helix in the beam direction was measured using our regular extinction measurement procedures [5,7], the absolute magnitudes of which are depicted in our standardized P,Q plot, Figure 1. Such a P,Q plot is a cartesian display of complex scattering amplitude S(0) versus particle orientation angles (χ,ψ) in the beam; where χ is the angle between the particle axis and the incident $\vec{k}$ vector, and ψ is the azimuth angle of the axis around $\vec{k}$. P and Q coordinates represent the in phase and 90°-out-of-phase components of the forward-scattered wave, respectively, with respect to the incident wave; and are calibrated so that

$$P = \frac{4}{x_v^2} |S(0)| \cos \phi(0), \qquad Q = \frac{4}{x_v^2} |S(0)| \sin \phi(0) ;$$

$\phi(0)$ is the phase lag of the $\theta = 0$ scattered wave and x_v denotes the volume-equivalent size parameter of the helix. Q is the volume-equivalent extinction efficiency. Figure 1 shows two curves corresponding to when the helical axis was swept through 90° so that χ varied as $0 \leq \chi\ (5°) \leq 90°$, in two mutually orthogonal planes containing the incident $\vec{k},\vec{E}$ vectors ($\psi = 0$) and $\vec{k},\vec{H}$ vectors ($\psi = \pi/2$), respectively. A vector drawn from the P,Q origin to any orientation mark along these curves is the S(0) vector, whose tilt from the P-axis is $\phi(0)$ and whose projection onto the Q axis gives the extinction efficiency at that orientation of the helix. Thus, it is seen that among the three principal orientations marked by k, E, and H in Figure 1, the obscuration is the most efficient at k orientation where the helical axis is

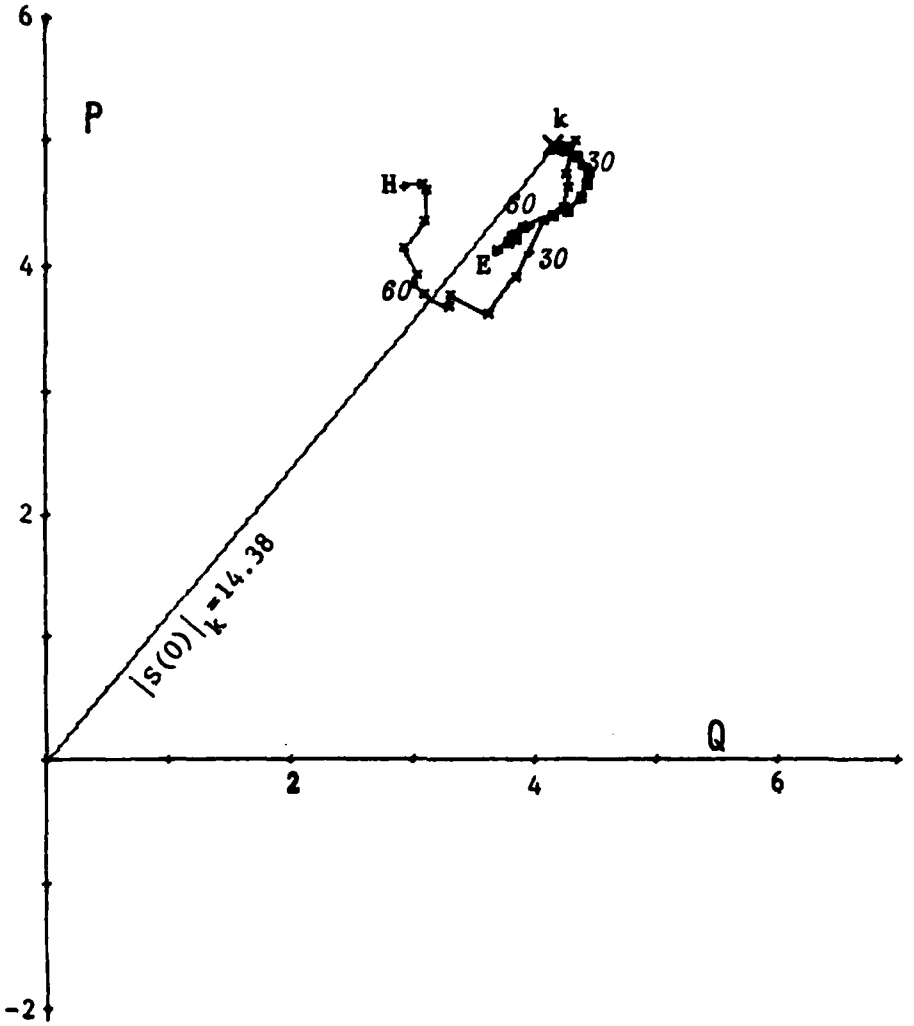

FIGURE 1. P,Q PLOT OF A 7-TURN RIGHT-HANDED HELIX

The cartesian display of the complex θ=0 scattering amplitude S(0) versus the orientation angles χ,ψ of a helix in the beam (See Sec. 2 for more details).
Target parameters: Diameter of rod = 0.48 cm; Length of rod = 79.9 cm; Volume = 14.40 cc; Surface area = 120.46 cm^2; Outer diameter of helix = 3.66 cm; Axial length = 4.35 cm. x_v = 2.979.; x_s = 6.111; Complex refractive index = 1.626-i0.012.
Volume equivalent extinction efficiency averaged over random orientations of the helix: $\overline{Q_{ext,v}}$ = 3.72.

aligned parallel to the beam, despite the fact that it presents the smallest geometrical cross section to the beam. A P,Q plot is thus seen to be a powerful way to visualize the subtle details of an extinction process as the particle rotates. If we assume the helix is approximately axisymmetric, we can also assess the extinction efficiency averaged over random orientations, $\overline{Q_{ext,v}}$ (see [5,7]). For this particular helix we found $\overline{Q_{ext,v}} = 3.72$). Finally, the scattering intensity i(0) at $\theta = 0$ is simply related to S(0) by $i(0) = |S(0)|^2$. We found $i(0)_K$=206.8, $i(0)_E$ = 152.0 and $i(0)_H$ = 148.6, respectively. Accuracy of $\theta = 0$ scattering measurements hinges most critically on the stability of the microwave background cancellation. This is especially true for this rather small-sized helix. Fortunately, we were able to make 3 or 4 runs in the early morning hours where the system was most stable and chose the best stabilized run according to the cancellation records kept in the computer diskette. Analysis of these records shows that the stability would not contribute more than 2% error in this particular measurement.

2.2 Angular Scattering Measurements $10° \leq \theta\ (10°) \leq 170°$.

Angular distributions of scattered radiation from the helix were measured in the above angular range of scattering angle θ for 3 combinations of transmitter-receiver antenna polarizations. The respective scattering intensities (in absolute magnitude) are denoted by i_{11}, i_{22} and i_{12}. i_{11} is the case when both antennas are polarized vertically, i_{22} is for both antennas polarized horizontal while i_{12}, the cross-polarized intensity, is for vertically polarized transmitter but horizontally polarized receiver. At each θ and antenna-polarization setting, the orientation of the helix in the beam was varied through 3 principal positions in the following sequence so its axis was oriented (a) vertical, (b) horizontal and parallel to incident $\vec{k}$, and (c) horizontal but perpendicular to $\vec{k}$. The results are shown graphically in Figure 2A for i_{11}; Figure 2B for i_{22}; and Figure 2C for i_{12} and $i_N = (i_{11} + i_{22} + 2i_{12})/2$ (total brightness of scattering for unpolarized light), respectively. Figure 2D then displays the θ dependence of the degree of linear polarization $P = (i_{11} - i_{22})/2i_N$. Data for each particle orientation in these figures are identified by symbols. For comparisons, Mie theory results for a sphere of the same volume and refractive index as the helix is also shown in each figure as a continuous curve. Figures 3A-3D are the duplicates of Figures 2A-2D, respectively, except that the former include interpolated data at $\Delta\theta = 5°$ via the Aitken-Lagrange cubic polynomial technique to facilitate the visualization of finer angular profiles. For this reason, data points in Figures 3A-3D are also connected by slashed curves.

Angular scattering patterns are intriguing and exotic but, due to their complexity, few theoretical analyses have been made except for listing a few outstanding features noted. Due to the rather small size of the helix compared to the large antenna-target separations (10.8 m between transmitter and target; 5.2 m between receiver and target), and hence the low scattered signal levels, significant measurement errors may exist due to the aforementioned compensation stability. Also, the system gain changes during the lengthy measurement runs may have contributed additional absolute-

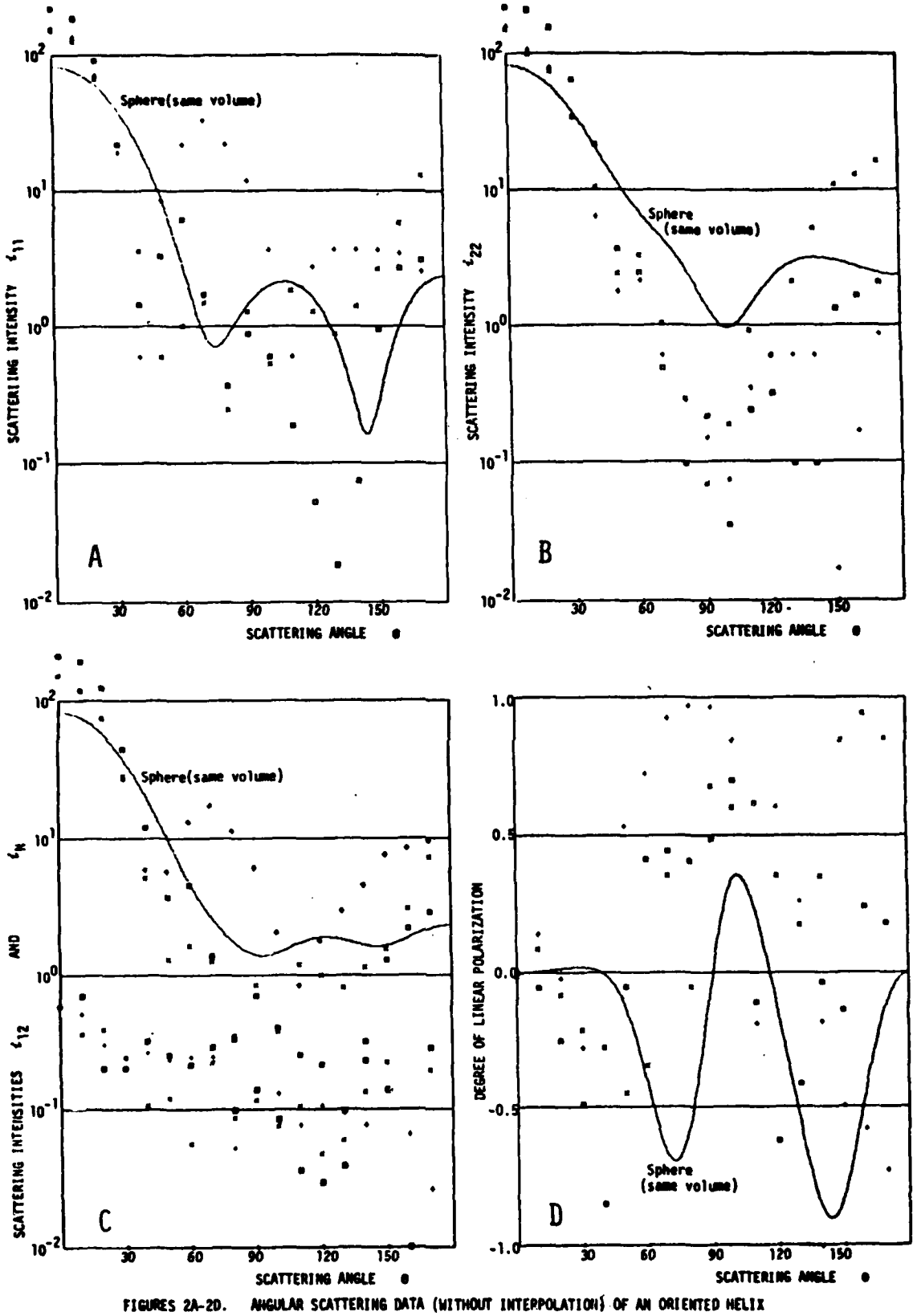

FIGURES 2A-2D. ANGULAR SCATTERING DATA (WITHOUT INTERPOLATION) OF AN ORIENTED HELIX

*The helix is a 7-turn, right-handed spiral made of a 79.9 cm-length acrylic rod. The detailed target parameters are: Volume=14.40 cc; Surface area=120.46 cm^2; x_v=2.979; m=1.626-i0.012; Diameter of acrylic rod employed=0.48 cm; Outer diameter of helix=3.66 cm; Axial length=4.35 cm.

*Orientation symbols: For i_{11} and i_{22}, + , x and □ denote respectively when the helical axis is parallel to the incident E, H and k vectors; while for i_{12} the same symbols except ■ instead of □ , are employed to identify the helix orientation in the beam. For i_N and Polarization plots, however, these symbols are used to denote when the axis is oriented vertical, horizontal (but perpendicular to the k vector), and horizontal (but parallel to the k vector), respectively.

*A continuous curve in each figure shows the Mie theory results for the equal-volume sphere possessing the same refractive index as the helix.

magnitude-calibration errors. Roughly estimated, the cumulative maximum errors would be about 5% if the absolute magnitudes of i_{11} and i_{22} are larger than 10^1, up to ~ 20% for those between 10^0 and 10^1, and may amount to as much as 100% for those absolute magnitudes having less than 10^{-1}.

(A) All i_{11}, i_{22} and i_{12} profiles, and hence the derived scattering profiles in i_N and P, are strongly dependent on the orientation of helix in the beam.

(B) The k-orientation, where the helical axis is aligned in the beam direction, exhibits the utmost variation in its profile. The strong peak near $\Theta = 0°$ and the deep trough near $\Theta = 130°$ differ by about 4 orders of magnitude for both i_{11} and i_{22}. As compared to scattering by an equal-volume sphere, this oriented helix casts stronger light near the beam ($\Theta \lesssim 30°$) and backward ($\Theta \gtrsim 160°$) directions, yet becomes practically invisible near $\Theta = 130°$ (Cf Figs. 3A-3C).

(C) When the helical axis was aligned parallel to the incident $\vec{E}$ vector, a wide conspicuous lobe was observed in its i_{11} profile, peaking at $\Theta = 70°$ (Figure 3A); yet such a lobe was absent in its i_{22} profile (Figure 3B). This marked lobe is responsible for the large positive polarization (>80%) in the angular range $65° \lesssim \Theta \lesssim 100°$ (Figure 3D).

(D) At all these 3 principal orientations, the helix scattered light with magnitude comparable to or even larger than by an equal-volume sphere near the beam ($\Theta \lesssim 30°$) and at the backward directions ($\Theta \gtrsim 160°$).

(E) Also, the cross-polarized scattering intensity i_{12} at these 3 principal orientations was unexpectedly low and became comparable to i_N only at the trough of scattering, $\Theta = 130°$. This suggests that at these principal orientations the helix approximated the scattering properties of an axisymmetric particle; i.e., $i_{12} = 0$ by virtue of symmetry. The accuracy of the i_{12} measurement is rather questionable, however, due to its low signal level (almost comparable to the level of uncompensated residual background).

(F) It is still premature to assess the integrated scattering properties over all scattering angles, such as the efficiencies of scattering, absorption and radiation pressure for the oriented helix. However, we can estimate with reasonable certainty that the asymmetry factors of scattering were 0.49, 0.86 and 0.77, respectively, when the helical axis was oriented vertically but perpendicular to the beam, parallel to the beam, and horizontally but perpendicular to the beam. Thus, when the axis is aligned to the beam, scattering is mostly confined in the forward directions ($\Theta \lesssim 90°$).

3. SUMMARY AND FUTURE RESEARCH SUGGESTIONS

The first scattering measurement on a single, penetrable helix whose overall size is comparable to the incident wavelength has been reported. The result was more exotic than was previously thought: (A) Perhaps the most

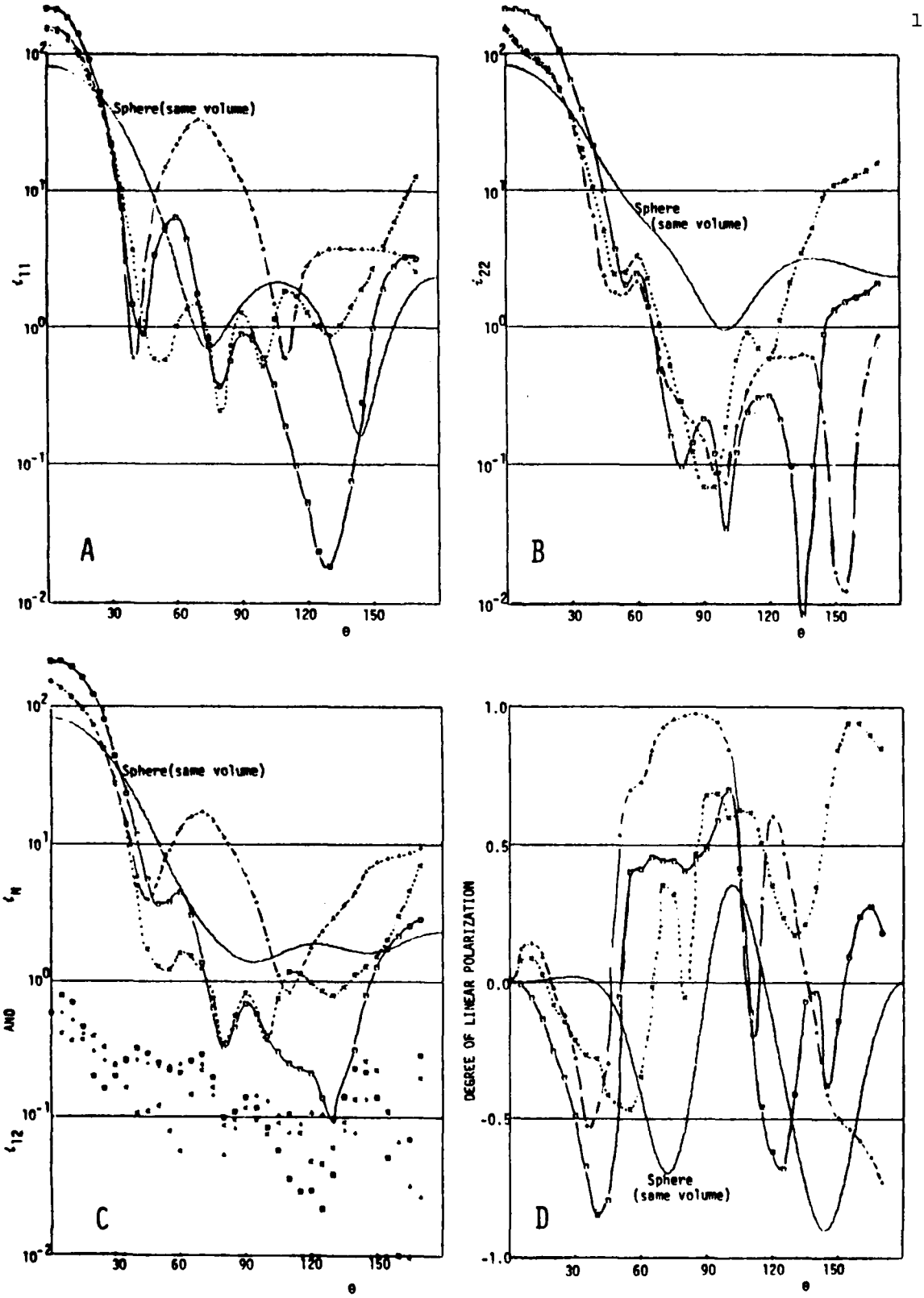

FIGURES A- D. ANGULAR SCATTERING DATA ($\Delta\theta = 5^\circ$ INTEPPOLATION) OF AN ORIENTED HELIX

*The helix is a 7-turn, right-handed spiral made of a 79.9 cm-length acrylic rod. The detailed target parameters are: Volume=14.40 cc; Surface area=120.46 cm^2; x_v=2.979; m=1.626-i0.012; Diameter of acrylic rod employed=0.48 cm; Outer diameter of helix=3.66 cm; Axial length=4.35 cm.

*Orientation symbols: For i_{11} and i_{22}, + , x and □ denote respectively when the helical axis is parallel to the incident E, H and k vectors; while for i_{12} the same symbols except ■ instead of □ , are employed to identify the helix orientation in the beam. For i_N and Polarization plots, however, these symbols are used to denote when the axis is oriented vertical, horizonatal (but perpendicular to the k vector), and horizontal (but parallel to the k vector), respectively.

*A continuous curve in each figure shows the Mie theory results for the equal-volume sphere possessing the same refractive index as the helix.

intriguing scattering exhibited by this particular helix was when its axis was aligned parallel to the incident beam; strongly peaked scattering was observed near $\theta = 0°$ and 170°, with a deep trough occuring near $\theta = 130°$. Also, the extinction cross section was near its maximum despite the geometric cross section which was at its minimum. The cross-polarized intensity i_{12} was low, however, contrary to what we expected for a larger magnitude due to the possible rotation of the plane of polarization of the scattered wave. (B) Similar strong scatterings near $\theta = 0°$ and at backscatter angles were also observed when the helix was oriented in the two other principal orientations. In addition, there is a prominently peaked, wide i_{11} lobe around $\theta = 70°$ when the helical axis was aligned parallel to the incident electric vector. (C) The angular scattering profiles as well as the $\theta = 0$ P,Q plot, are highly exotic in the sense that they are markedly different from those by other appropriately sized particles, spherical or nonspherical.

The helix was rather small in its rod diameter. This fact, along with the observed strong forward scattering, suggests an explanation of the observed angular profile based on the Rayleigh-Gans-Debye approximation theory, by subdividing the helix into small, cylindrical disk sections and adding the contribution from each section to assess the net scattering.

Due to the small helix size and perhaps the insufficient system stability, the angular scattering data may contain appreciable errors, especially when the signal level is low. We expect that this can be significantly improved in the near future when our on-going instrumentation upgrade is completed. We may then extend the measurement to cover other orientations or even assess the random-orientation averages without sacrificing measurement accuracy.

Circular intensity differential scattering (CIDS) measurements cannot now be made. A plan is underway to incorporate devices for amplitude-phase measurements and/or circular polarization into our facility.

LITERATURE CITED

1. Lakhtakia, A., Varadan, V.K. and Varadan, V.V., Appl. Opt. 24, 4146 (1985).

2. Patterson, C.W., Singham, S.B. and Salzman, G.C., CIDS of Light by Hierarchical Molecular Structures (submitteed to J. Chem. Phys. from Los Alamos National Laboratory, 1985).

3. Roberts, S. and von Hippel, A., J. Appl. Phys. 17, 610 (1946).

4. Schuerman, D.W. and Wang, R.T., Army CSL Contractor Rept., ARCSL-CR-81003 (1981).

5. Wang, R.T. in "Proc., 1983 CRDC Conference," J. Farmer and R.H. Kohl, eds., Army CRDC-Sp-84009, pp. 223-235 (July, 1984).

6. Wang, R.T., and Gustafson, B.A.S., in the same "Proceeding" as above [Ref. 5] pp. 223-235 (July, 1984).

7. Wang, R.T., in "Proc., 1984 CRDC Conference," R.H. Kohl and D. Stroud, eds., Army CRDC-85007, pp. 315-326 (June 1985).

END

12-86

DTIC